Talanta 98 (2012) 69–78

Contents lists available at SciVerse ScienceDirect

Talanta

journal homepage: www.elsevier.com/locate/talanta

Optical detection/collection of toxic Cd(II) ions using cubic Ia3d aluminosilica mesocage sensors

Sherif A. El-Safty [a,b,*], Mohamed A. Shenashen [a], Mohamed Khairy [a,b]

[a] National Institute for Materials Science (NIMS), Exploratory Materials Research Laboratory for Energy and Environment, 1-2-1 Sengen, Tsukuba-shi, Ibaraki-ken 305-0047, Japan
[b] Graduate School for Advanced Science and Engineering, Waseda University, 3-4-1 Okubo, Shinjuku-ku, Tokyo 169-8555, Japan

ARTICLE INFO

Article history:
Received 22 May 2012
Received in revised form
15 June 2012
Accepted 18 June 2012
Available online 4 July 2012

Keywords:
Cubic Ia3d
Sensors
Optical
Cadmium
Removal
Detection

ABSTRACT

Optical sensors for selective removal and detection of extremely toxic ions such as cadmium (Cd^{II}) in aquatic samples were successfully fabricated via simple strategy. Aluminosilica-based network platforms are used as selective mesopore shape and size carriers in order to fabricate optical sensors through the direct functionalization of α, β, γ, and δ-tetrakis(1-methylpyridinium-4-yl)porphine ρ-toluenesulfonate (TMPyP) moieties without any prior surface modification using silane or thiol agents. In turn, the key advantage of a heretical three-dimensional (3D) cubic Ia3d mesocage is the facile access of target ions such as ion transports and the high affinity responses of TMPyP receptor-Cd(II) analyte binding events, which result in the easy generation and transduction of optical signals even at the trace level of the Cd(II) ion. The optical sensor design-based aluminosilica cages enable the sensitive detection and selective removal of Cd(II) ions even at ultra-trace concentrations of 10^{-10} mol/dm^3 with rapid response time (in minutes). This rational strategy is crucial to the development of optical mesocollectors (i.e., probe surface-mounted naked-eye ion-sensor strips) with highly selective Cd(II) ion removal from aqueous water. These new classes of optical mesocollectors exhibit long-term stability and reusability of deleterious Cd(II) ions, which makes them efficient for various analytical applications.

© 2012 Elsevier B.V. All rights reserved.

1. Introduction

Heavy metals and numerous other toxic compounds are present in the environment. These heavy metals and toxic compounds may contaminate our water supplies, particularly in industrial areas. They are components in the clothes we wear, the paints used on houses, as well as the machines we use at the workplace and in all modern office environments [1–5]. Heavy metals are materials in many of the simple items that exist in the modern world. In particular, large quantities of cadmium ions are present in the domestic environment; these ions are components in several of the most commonly utilized toxic metals in the world. Cadmium is a soft, silver–white non-essential element with an average crustal concentration of (0.1–0.2) mg/kg (0.89–1.78 μmol/kg), which negatively affects plant growth and development. It is released into the environment by power stations, heating systems, metal-working industries, or urban traffic [6–8]. This element is widely used in electroplating, pigments, fertilizers, plastic stabilizers, Ni–Cd batteries, and metal plating. Cadmium is mainly sourced from the burning of fossil fuels such as coal or oil, the incineration of municipal waste, the application of phosphate fertilizers or sewage sludge to farm fields, and smoking. Therefore, food and smoking are the largest sources of cadmium exposure (Smokers have approximately twice the cadmium content in their bodies compared with nonsmokers). The reference dose for cadmium in drinking water is 0.0005 ppb per day. The acute (short-term) effects of cadmium in humans through inhalation exposure consist mainly of effects on the lung, such as pulmonary irritation [6,9,10]. Chronic (long-term) inhalation or oral exposure to cadmium leads to a calcium build-up in the kidneys, which can cause kidney disease including proteinuria, a decrease in glomerular filtration rate, and an increased frequency of kidney stone formation. Cadmium is shown to be a developmental toxicant in animals, which results in fetal malformations and other effects. However, no conclusive evidence regarding its effects as a developmental toxicant in humans exists. The chronic inhalation or oral exposure of animals to cadmium affects the kidney, liver, lung, bone, immune system, blood, and the nervous system. An association between cadmium exposure and an increased risk of lung cancer is reported from human studies, but these studies are inconclusive due to confounding factors. Animal studies demonstrate an increase in lung cancer because of

* Corresponding author at: National Institute for Materials Science (NIMS), Exploratory Materials Research Laboratory for Energy and Environment, 1-2-1 Sengen, Tsukuba-shi, Ibaraki-ken 305-0047, Japan. Tel.: +81 298592135; fax: +81 298592025.
E-mail addresses: sherif.elsafty@nims.go.jp, sherif@aoni.waseda.jp (S.A. El-Safty).

0039-9140/$ - see front matter © 2012 Elsevier B.V. All rights reserved.
http://dx.doi.org/10.1016/j.talanta.2012.06.046

a long-term inhalation exposure to cadmium. The EPA classifies cadmium as a Group B1, which means it is a probable human carcinogen. The World Health Organization (WHO) and the Environmental Protection Agency (EPA) recommend a (3.0–5.0) $\mu g\,L^{-1}$ [9–11] standard for Cd(II) in drinking water.

Two key factors should be considered for the sensing system: receptors and an immobilization/ transducing platform. The receptors are responsible for the selectivity, and the immobilization/ transducing platform is responsible for sensor stability as well as sensitivity, which depends on the technique used (optical, electrochemical, etc.). The sensing methods capable of quantifying these trace elements at low levels, including atomic absorption spectroscopy and inductively coupled plasma (ICP) combined with atomic emission spectrometry (ICP-AES) or with mass spectrometry (ICP-MS), are of great interest. The ICP-MS technique is a powerful method owing to its multi-element capacity and high sensitivity [10–12]. Other sensing methods include electrochemical, neutron activation, flame atomic fluorescence spectrometry, molecular absorption spectrometry, and X-ray fluorescence. The majority of these methods actually provide analytical devices and assays that are capable of detecting and quantifying trace metal ion concentrations. However, these devices are normally restricted to wealthier hands with limited access to pollution monitoring agencies and other research organizations in developing countries. A low-cost, easy-to-use, and reliable device is still greatly needed for environmental monitoring and green chemistry. The development of optical collectors for the detection of hazardous trace metals is of great interest in the environmental and biomedical fields [10–13].

Nanometer-sized materials with engineered features, including size, shape, composition, and function, play a leading role in detection/removal design because of their emerging applications in the optical detection of cations and anions [13–15]. Ordered mesoporous silica monoliths featuring uniformly sized, monodispersed porosities in the range of (2–20) nm and large particle sizes show promise as a new class of optical sensor material. Successful nanosensor designs allow scientists to develop controlled assessment processes for the naked-eye detection of several toxic heavy metal ions up to nanomolar concentrations [14]. Nonetheless, creating smart detection, eco-friendly solid sensors with low cost and simple fabrication for Cd(II) ions in basic laboratory assays remains a challenge. Since the discovery of a novel class of the M41S family of mesoporous molecular sieves, the incorporation of aluminum into the framework has provided materials with acidic active sites [16–18]. These aluminosilica materials show an exciting range of applications despite the existence of a structural disorder similar to those in amorphous alumina and aluminosilicas [17,19]. High aluminum content in frameworks can lead to increases in the acidity of the resultant solid acid aluminosilica materials. However, the ordering and hydrothermal stability of these materials are drastically decreased at low Si/Al ratios [20–22]. Alumina/ aluminosilica materials are one of the most widely used materials in heterogeneous catalysis because of its unique catalytic, adsorption, optical, and electronic properties [23–28]. For the first time, the key features and advantages of the mesostructured aluminosilica-based carriers of receptors can be effectively used for the simple fabrication and design of low-cost probe surface-mounted naked-eye ion-sensor strips [see for instance [29–32]].

In this paper, real evidence is presented of the successful design of a nanosensor/collector based on cubic Ia3d aluminosilica mesocage cavities for the colorimetric recognition and removal of Cd(II) ions. The use of aluminosilica-based three-dimensional (3D) platforms as selective mesopore shape and size carriers leads to a simple fabrication of optical sensors through the direct functionalization of the TMPyP chelate without a previous modification of their pore surfaces. The optical sensor design-based aluminosilica cages enables the sensitive detection and selective removal of Cd(II) ions even at ultra-trace concentrations of 10^{-10} mol/dm^3 with a rapid response time (in minutes). These new classes of optical mesocollectors allow the development of probe surface-mounted naked-eye ion-sensor strips with highly selective removal of Cd(II) ions from aqueous water and waste disposal samples.

2. Experiments

2.1. Chemicals

All materials were analytical grade and used as purchased without further purification. Tetramethylorthosilicate (TMOS), aluminum nitrate enneahydrate ($Al(NO_3)_3.9H_2O$), Pluronic F68 ($EO_{80}PO_{27}EO_{80}$, $M_{av}=8400$) surfactant and α, β, γ, δ-tetrakis (1-methylpyridinium-4-yl)porphine ρ-toluenesulfonate (TMPyP) were obtained from Sigma-Aldrich Company Ltd., USA.

2.2. Synthesis of cubic Ia3d aluminosilica mesocages

Cubic Ia3d aluminosilica mesocage was fabricated by using direct templating method of lyotropic liquid crystalline phase of F68 as template (see Table 1). In typical conditions, the composition mass ratio of F68: TMOS: HCl/H_2O was 1:2:1 respectively. To obtain samples with aluminum contents at Si/Al ratio of 9, 4, 1.5 and 1, the composition of $Al(NO_3)_3.9H_2O$ was varied. For example, in the direct synthesis of aluminosilica monoliths at Si/Al mole ratio of 4 and at F68/TMOS mass ratio of 0.5, the precursor solution (0.45 g of F68 surfactant, 0.9 g of TMOS, 0.256 g of $Al(NO_3)_3.9H_2O$, and 1.125 g of H_2O-HCl (pH 1.3)) was used. Homogeneous sol–gel synthesis was achieved by mixing F68/TMOS/$Al(NO_3)_3$ in a 100 cm^3 beaker and then shaking at 50 °C for 2 min until homogeneous. The exothermic hydrolysis and condensation occurred rapidly by addition of acidified aqueous solution of HCl (at pH = 1.3) to this homogeneous solution. The resulting an optical gel-like material was put in a graduate ingot and acquired the shape and size of the cylindrical casting vessel. The resultant surfactant/aluminosilica solid was gently dried at room temperature for 3 h and allowed to stand in a sealed container at 25 °C for 1 day to complete

Table 1
Synthesis conditions as well as structural and textural parameters of cubic mesocage aluminosilica monoliths fabricated using the lyotropic phases of F68 as soft templates with a wide range of Si/Al mole ratios.

Si/Al mole/mole	Synthesis conditions			Structural parameters			
	10^2.TMOS/mole	(10^3) Al $(NO_3)_3$/ mole	F68/TMOS w/w	a^* nm	S_{BET} m^2/g	Dp nm	Vp cm^3/g
9	1.31	1.36	0.5	20.1	705	6.0	0.91
4	1.31	3.4	0.5	20.5	607	6.2	0.81
1.5	1.31	9.1	0.5	20.9	420	6.8	0.71
1.0	1.31	13.6	0.5	21.2	350	7.1	0.56

* Cubic unit-cell constant ($a=2d_{100}/\sqrt{3}$).

the drying process. The organic moieties were then removed by calcination at 550 °C for 7 h (Table 1).

2.3. Fabrication design of optical aluminosilica mesocage collectors

Cubic Ia3d aluminosilica mesocage was fabricated by the direct immobilization of and ethanol solution/10 mg TMPyP probe into 0.5 g Cubic Ia3d aluminosilica mesocage carriers. The impregnation procedure was performed under vacuum at 25 °C until probe saturation was achieved. The ethanol was removed by a gentle vacuum connected to a rotary evaporator at room temperature, leading to the direct contact of the dye probe into the mesoporous aluminosilica. The immobilization process was repeated several times until the equilibrium adsorption capacity of the TMPyP-probe reached saturation. The resulting mesoporous aluminosilica sensor was thoroughly washed with deionized water until no elution of TMPyP color was observed. The sensors were dried at 60 °C for 2 h [29,30].

The adsorption capacity (Q, mmol g^{-1}) of TMPyP into aluminosilica monoliths at saturation was determined by the following equation: $Q=(C_o-C)$ V/m, where Q_t is the adsorbed amount at saturation time t, V is the solution volume (L), m is the mass of the aluminosilica monolithic carriers (g), and C_o and C are the initial and saturation concentrations at time t, respectively (Table 2).

2.4. Analyses of ultra-traces level of Cd(II) ions

The colorimetric determination and visual detection of Cd(II) analyte by using TMPyP probe-doped cubic Ia3d mesocage aluminosilica was carried out by adding a mixture containing specific concentrations of each analyte ions adjusted at pH ca. 2 (by using 0.2 M of KCl/HCl/H_2SO_4), pH 4 (by using 0.2 M CH_3COOH/CH_3-COONa), and pH 7 (by using 0.2 M of 3-morpholinopropane sulfonic acid, MOPS), respectively, to ~10–20 mg of the cubic Ia3d mesocage aluminosilica nanosensors at constant volume (20 cm^3) with shaking. After an interval of time, the nanosensors were collected by using suction and 25 mm-diameter cellulose acetate filter paper (Sibata filter holder). The color of the collected sample was estimated by the naked-eye and UV–vis spectrometry. In order to quantitative record the change in the reflection spectra of the sensors/collectors by addition of the Cd(II) ions using solid-state UV–vis spectrophotometer (a Shimadithizoneu 3700 model solid), the aluminosilica nanosensors were grinded to fine powder disk to observe the homogeneity in the reflectance spectra. Our previous studies revealed that the monolith-based sensor in the grinded form did not loss its utility or functionality in terms of fast response-time and sensitivity [13].

The concentration of Cd(II) ions was analyzed by using a Seiko SPS-1500 inductively coupled plasma atomic emission spectrometer (ICP-AES) before and after detection/removal. To ensure both accuracy and precision of the analyte ion sensing system, successive measurements were carried out using wide-range concentrations of the standard "well-known" solutions of analyte ions.

The stoichiometry of $[Cd\text{-}TMPyP]^{n+}$ complexes was determined from a Job's plot, in which changes in the absorbance of the color complexes in solution under experimental control conditions were monitored. The M: TMPyP stoichiometric ratio of the $[Cd(II)\text{: }TMPyP]^{n+}$ complexes was determined to be 1:1 during this sensing assays. The detection limit (LOD) of Cd(II) analyte ions by using the aluminosilica sensors was estimated from the linear part of the calibration plot [13a,30], according to the equation $D_L=kS_b/m$, where $k=3$, S_b is the standard deviation for the blank, and m is the slope of the calibration graph in the linear range.

2.5. Analysis Cubic Ia3d aluminosilica collector

N_2 adsorption–desorption isotherms were measured using a BELSORP MIN-II analyzer (JP. BEL Co. Ltd) at 77 K. The pore size distribution was determined from the adsorption isotherms by using nonlocal density functional theory (NLDFT). Specific surface area (S_{BET}) was calculated using multi-point adsorption data from linear segment of the N_2 adsorption isotherms using Brunauer-Emmett-Teller (BET) theory. Before the N_2 isothermal analysis, all prepared samples were pre-treated at 200 °C for 8 h under vacuum until the pressure was equilibrated to 10^{-3} Torr.

High-resolution transmission electron microscopy (HRTEM), scanning transmission electron microscopy (STEM), and energy dispersive X-ray spectroscopy for elemental mapping (STEM-EDS) were performed using a JEOL JEM model 2100 F microscope. HRTEM was conducted at an acceleration voltage of 200 kV to obtain a lattice resolution of 0.1 nm. The HRTEM images were recorded using a CCD camera. STEM and STEM-EDS were carried out at a camera length of 80 cm and a spot size of 1 nm. In the HRTEM, STEM, and STEM-EDS characterization, the solid sample was dispersed in ethanol solution using an ultrasonic cleaner, and then dropped on a copper grid. Prior to inserting the samples in the HRTEM column, the grid was vacuum dried for 20 min.

Small angle powder X-ray diffraction (XRD) patterns were measured by using a 18 kW diffractometer (Bruker D8 Advance) with monochromated CuKα radiation and with scattering

Table 2
The effect of Si/Al ratios of cubic Ia3d aluminosilica mesostructures on Cd(II) ion-sensor/collector functionalities in terms of accessibility, sensitivity, response time, and reversibility features.

Sensor with Si/Al	Q [mmol g^{-1}]	Sensing conditions		Optical sensing/collecting features		Collector featured with reuse cycles			
		t_R min	pH range	LOD mol dm^{-3}	D_R mol dm^{-3}	Eluant 0.1 M	No.*	t_R min	E%
9	0.07	3	8–10.5	3.08×10^{-8}	8.8×10^{-10} to 8.8×10^{-7}	EDTA	2	3	98
							4	3	96
							6	4	94
4	0.08	3	8–10.5	3.8×10^{-8}	8.8×10^{-10} to 8.8×10^{-7}	EDTA	2	3	98
							4	4	96
							6	4	94
1.5	0.092	3	8–10.5	4.2×10^{-8}	2×10^{-9} to 8.8×10^{-7}	EDTA	2	4	98
							4	4	95
							6	5	94
1	0.12	3	8–10.5	7.5×10^{-8}	1.12×10^{-9} to 1.0×10^{-6}	EDTA	2	4	98
							4	5	96
							6	6	85

* Number of reuse cycles; E%: efficiency of the collector within the reuse cycles.

reflections recorded for 2θ angles between 0.1° and 6.5° corresponding to d-spacing between 88.2 and 1.35 nm. First, the powder samples were ground and spread on a sample holder. The samples were scanned in the range from 2θ=0.1°–6.5° with step size of 0.02°. To confirm the resolution of the diffraction peaks with standard reproducibility in 2-theta ($\pm$0.005), the sample measurement was recorded by using both graphite monochromator and Göbel mirror detectors. Both detectors were used to generate focusing beam geometry and parallel primary beam. The sample measurement was repeated three times under rotating at various degrees (15°, 30° and 45°).

^{27}Al Magic-angle spinning nuclear magnetic spectroscopy (^{27}Al MAS NMR) was also recorded using a Bruker AMX-500 spectrometer. ^{27}Al NMR spectra were measured at a frequency of 125.78 MHz with a 90° pulse length of 4.7 μs. For all samples, the repetition delay was 64 s with a rotor spinning at 4 kHz for ^{27}Al NMR. The chemical shift scale was externally adjusted to be zero for ^{27}Al signal by using aqueous solution (1 N) of $Al(NO_3)_3$. To investigate the acidic properties of aluminosilica samples, NH_3 temperature-programmed desorption (NH_3-TPD) was measured by using a BEL-Japan TPD-1 S system with a quadrupole mass spectrometer.

3. Results and discussion

3.1. Fabrication of cubic Ia3d aluminosilica mesocage collectors

The nanosensors were successfully fabricated using a direct grafting process, in which the TMPyP probe was immobilized into cubic Ia3d aluminosilica monoliths without previous modification of their pore surfaces (Scheme 1A, B). This direct immobilization enabled the design of uniformly cubic Ia3d chemosensors without pore blockage, which allows the highly selective targeting of cations such as Cd(II) ions [26,27,33,34]. This collector shows evidence of sensing responses in terms of sensitivity, selectivity, and response time of the TMPyP probe chemosensors, which are induced by receptor "molecular probe"–Cd(II) analyte binding events (Scheme 1C) [35,36]. The direct immobilization of hydrophobic TMPyP-probe molecules with a high adsorption capacity into the cage cubic Ia3d aluminosilica led to the design of optical molecular sensors for the simple detection/removal of ultra-trace levels of Cd(II) ions. A particularly important feature of the 3D Ia3d aluminosilica mesocage is the potential functionality of active sites, which leads to the high accessibility and adsorption capacity of the TMPyP chelate [37]. Al MAS NMR spectra indicated that the incorporation of Al into mesoporous frameworks leads to the formation of the aluminum species' coordination state in four-, five-, and six-coordinate environments at chemical shifts of (−1, 37, and 58) ppm, respectively (Fig. S1). The coordination and location of aluminum sites in the frameworks are key determinants in the generation of the aluminosilica samples' surface acidity. The surface acidity of the aluminosilica monoliths is evidenced by the two resultant peaks of NH_3 desorption at approximately 200 °C, and a small, broad peak at about (200–500) °C (Fig. S2). The results clearly indicate that the ammonia is desorbed from the weak Lewis and mildly strong Bronsted acid sites of the OH^- groups of the aluminosilica carriers [34].

The direct-templating strategy controlled the cubic mesostructured aluminosilica with a wide range of Si/Al ratios of $9 < Si/Al < 1.0$ using [F68/$Al(NO_3)_3$/TMOS/acidified H_2O] composition phases acidified H_2O (Table S1). The XRD pattern (Fig. 1A-a) of the aluminosilica carriers shows well-resolved Bragg peaks of cubic Ia3d structures. Despite the high loading level of the TMPyP probe moieties into the necked pore channels or onto the pore surface, finely resolved Bragg diffraction peaks are evident for the cubic Ia3d cubic mesocage geometries (Fig. 1A-b). The N_2 isotherms revealed the uniformity and regularity of the 3D cubic cage nanosensors, as shown by a well-known sharp inflection of adsorption/desorption branches (Fig. 1B). However, an H2-type hysteresis loop and the well-defined steepness

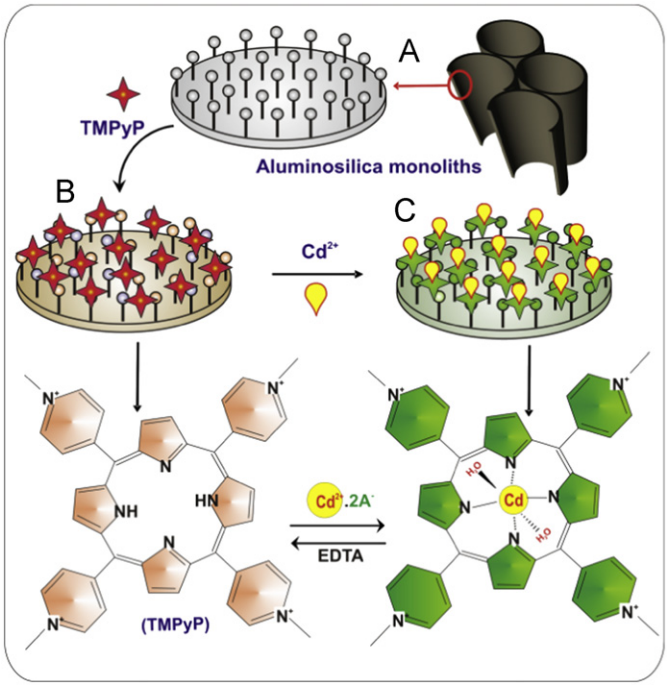

Scheme 1. Schematic model of the mesocage aluminosilicate nanosensor/collector design through the direct dispersion of TMPyP chelate and the sensing recognition of Cd(II) ions.

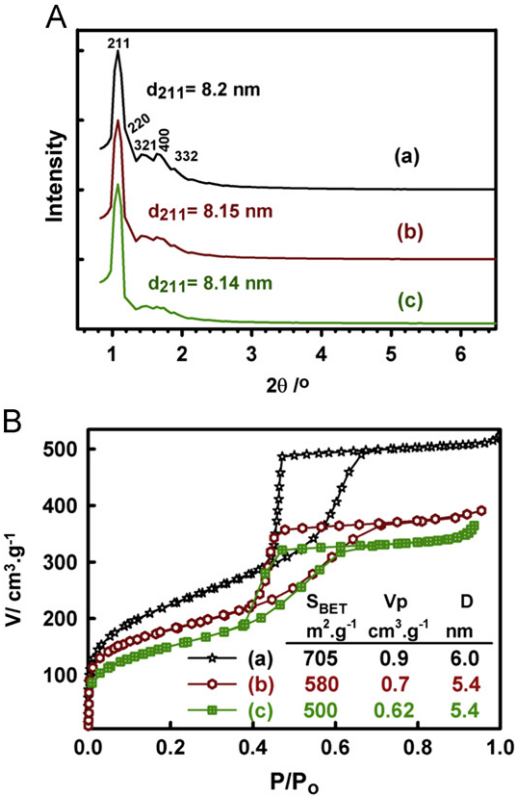

Fig. 1. XRD patterns (A) and N_2 isotherms (B) of optical collectors (b) fabricated by the immobilization of the TMPyP chelate into cage cubic Ia3d aluminosilica monoliths (with Si/Al mole ratios of 9) (a), and after three reuse cycles (c).

of the isotherms indicate that uniform, cage-like pore structures are characteristic of the cubic Ia3d mesocollector [26,27,38]. A characterization analysis of the mesocaptor revealed three key features. First, the addition of large amounts of aluminum salt to the synthesis composition domains influence the increases in micellar aggregate sizes and volume fractions, which cause the unit-cell constants and pore sizes of Ia3d cubic structures to increase (Table 1). Second, although N_2 isothermal data indicate that the organic moieties might incorporate into the inner pores, a significant amount of organic moieties is mainly anchored in the pore surfaces, which leads to a high flux and a rapid diffusion of analtyes. Third, uniformly shaped pore geometries and textural properties of cubic Ia3d mesocollectors are attained. Such a retention in mesostructural integrity led to rational optical mesocollector designs, as evidenced by the high selectivity and sensitivity of the Cd(II) target ions with rapid response time (3 nm) [26,27,39].

Transmission electron microscopy (TEM) images (Fig. 2) reveal well-organized mesopore arrays over a large area of the mesocollectors' cubic Ia3d lattices, despite the immobilization methods of the loading coverage of bulky chromophore molecules, such as the TMPyP probes, into mesoporous aluminosilica monoliths. The TEM images (Fig. 8) show uniformly sized pores and continuous spherical arrangements along the [311], [111], [100], and [110] zone axes of the cubic Ia3d mesocollectors [37,40]. In general, the TEM patterns (Fig. 2) reveal the retention of uniformly shaped cubic Ia3d geometries of collectors, which lead to the intrinsic mobility and high flux of the Cd(II) analyte ions during the binding with TMPyP probe molecules. Dark fields in the STEM image (Fig. 3A) confirm the formation of nanoscale collector particles. The particle morphology and the EDS mapping of mesocollector were further characterized using STEM and STEM-EDS (Fig. 3b–e). The STEM-EDS map of the aluminosilica mesostructure collectors exhibits the presence of Si, Al, O, C, and N (Fig. 3). Contributions of O, Si, and Al come mainly from the mesostructure. The STEM-EDS map also indicates that C, N, and S atoms of the TMPyP chelate are uniformly distributed throughout the mesoporous aluminosilica, thus allowing the homogenous diffusion of metal ions toward the TMPyP molecular probe centers [41].

3.2. Cubic Ia3d aluminosilica mesosensor for visual removal and detection of Cd(II) ions

In this study, a series of batch contact-time experiments was performed to define and evaluate systematically the suitable conditions of the Cd(II) ion-mesosensor. The quantification procedure of Cd(II) ion-sensing with a cubic Ia3d aluminosilica mesocage sensor fabricated with Si/Al ratios of 9, 4, 1.5, and 1, respectively, was studied after equilibration and response times (t_R) of 3 min (Table 2). The prominent color change and signal saturation in the reflectance spectra of mesosensors were recorded after the t_R, which can be considered as a reference signal. The results show that the t_R values of the Cd(II)-ion collectors are sufficient to achieve good color separation "signal" between the collector "blank" and the Cd(II) ion-sensing "sample," even at low recognition or trace concentration-levels of the Cd(II) metal. The results show that the charge transfer between the Cd(II) ions and the TMPyP-probe occurred within a short time period ($\sim$3 min) in all the 3D aluminosilica sensor systems (Table 2), despite the effect of high or low aluminum content in the sensor matrices.

In solid-state ion-sensing systems, the aluminosilica collector is strongly sensitive in terms of its optical "color intensity" and signal responses toward the pH of the analyte solution [42]. To define and evaluate systematically the suitable pH conditions for donor–acceptor combinations between solid modified-TMPyP and metal targets, the reflectance spectra of the $[Cd\text{-}TMPyP]^{n+}$ complexes on pore surfaces were carefully monitored over a wide range of pH solutions (Fig. 4). The optimum change in color intensity of the $[Cd\text{-}TMPyP]^{n+}$ complexes was around pH 9.5 for the Cd(II) ions. The pH graph suggests that the Cd(II) ions can bind strongly to solid modified-TMPyP with high stability during the formation of octahedral $[Cd\text{-}TMPyP]^{2+}$ complexes at pH 9.5.

The design-made mesocollector/sensor shows that the colorimetric determination using UV–Vis reflectance spectroscopy can quantitatively validate the wider concentration range of the Cd ions (8.89×10^{-10} to 1×10^{-6} mol/dm^3) compared with the Cd(II) ion recognitions in the TMPyP solution at pH 9.5 (8.89×10^{-7} to

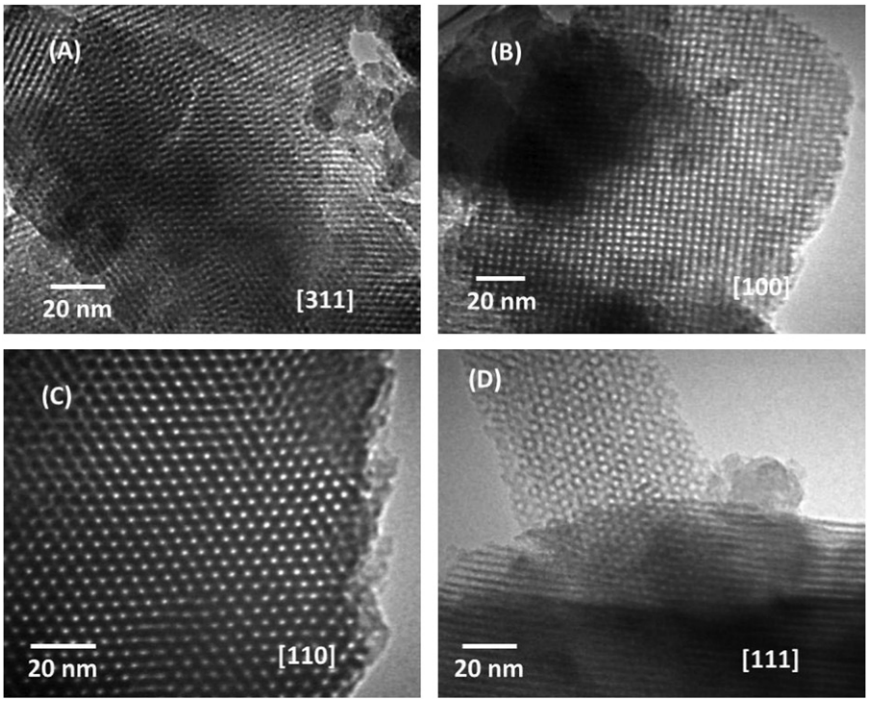

Fig. 2. TEM micrographs recorded along the (A) [311], (B) [100], (C) [110], and (D) [111] directions of the optical mesocage collector that was fabricated by the direct immobilization of TMPyP chelate into cubic Ia3d aluminasilica carriers with Si/Al mole ratios of 9.

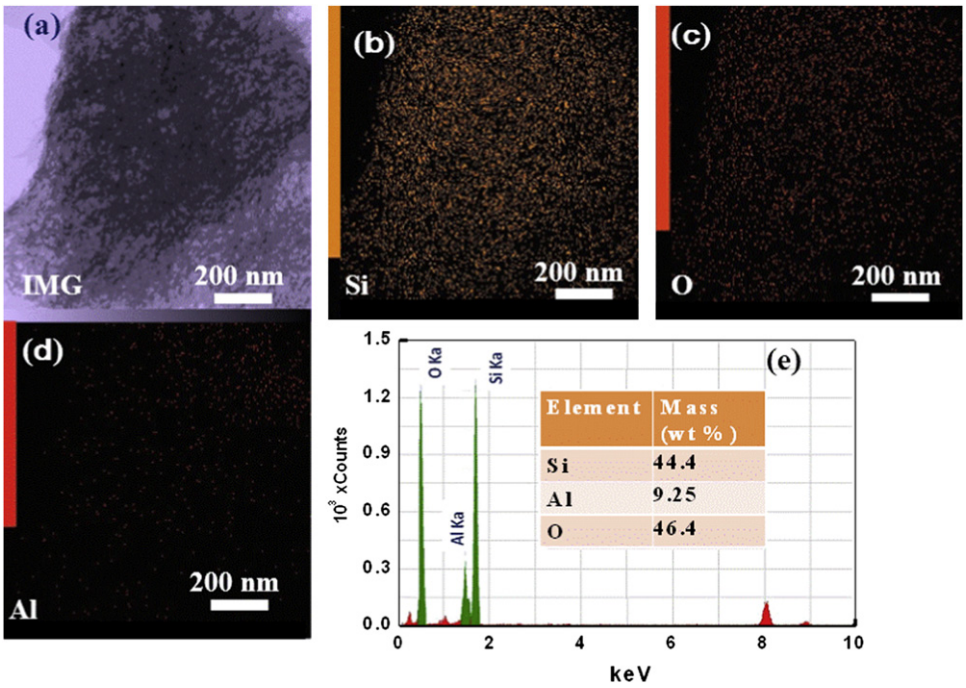

Fig. 3. STEM image, EDS, and STEM-EDS mapping of the mesoporous aluminosilica-TMPyP collector (with Si/Al ratio of 9) (a) STEM image, (b) silicon, (c) oxygen, (d) aluminum, (e) EDS analysis of atomic abundance of the mesocollector.

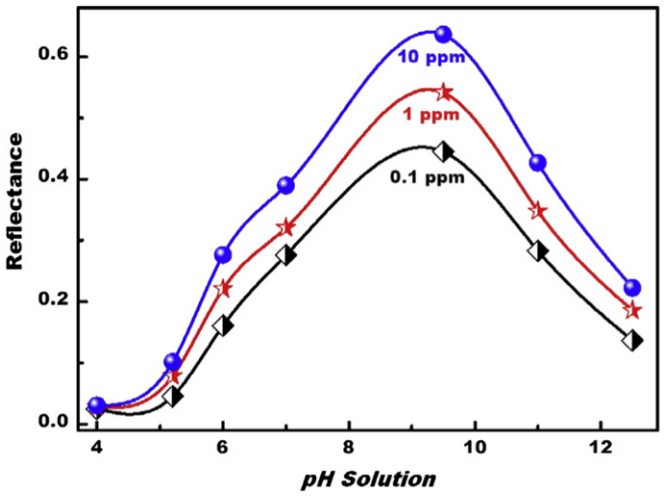

Fig. 4. Quantitative study of the pH collector responses based on the aluminosilica carriers fabricated with a Si/Al ratio of 9 at optimal sensing conditions of Cd(II) ion concentrations ($t_R > 3$ min, collector amount of 20 mg, volume of 20 mL, and temperature of 25 °C). The reflectance spectra of the $[Cd\text{-}TMPyP]^{n+}$ complexes was measured at λ_{max} of 620 nm.

1×10^{-5} mol/dm^3) [43]. The Cd(II) ion-quantification experiments (in TMPyP solution) were carried out in a quartz flask with a total volume of 20 mL. The Cd(II) aliquots were injected from a 200 ppm aqueous stock solution into a flask containing a mixture solution of 30 μM TMPyP at pH 9.5. Our finding indicated that in solid systems, naked-eye detection is clearly observed in a wider concentration range of (0.0001–20.0 ppm), as evidenced by the color change from yellow to green after the addition of Cd(II) ions (Table 2 & Fig. 5). The utility of the design-made aluminosilica-TMPyP collector also leads to a simple separation and visual detection over a wider, adjustable concentration range, as well as a sensitive quantification of Cd(II) analyte ions at trace levels ($\sim 3 \times 10^{-8}$ mol/dm^3). The key feature of the aluminosilica mesocage is that the separation and preconcentration of Cd(II) ions onto the aluminosilica pore surfaces are more flexible and sensitive even at trace concentration levels during the formation of Cd-to-TMPyP binding events, compared with optical sensors fabricated by using silica monoliths as carriers [40,13]. In general, the color change provides a simple procedure for the sensitive and selective detection/collection of Cd(II) ions without the need for sophisticated instruments (Fig. 5A).

As a result of the selective uptake of Cd(II) target ions with the TMPyP-modified aluminosilica collector (Fig. 5A), the reflectance spectra at λ_{max} of 620 nm was observed. However, the reflectance spectra of TMPyP-modified sensor at 645 nm were exhibited a blue shift to 620 nm as a resultant of charge transfer between the Cd(II) and TMPyP-probe during the formation the $[Cd\text{-}TMPyP]^{n+}$ complex.

The calibration plot of the aluminosilica mesocollector can be presented as a linear correlation at low concentration ranges of Cd(II) analyte ions (Fig. 5B). Specifically, the linear curves indicate that the metal analytes can be detected with high sensitivity over a wide concentration range. However, a nonlinear correlation at the inflection point is evident at the highest Cd(II) ion concentration. The quality of the calibration method is necessary to ensure both the accuracy and the precision of Cd(II) ion sensing systems. The detection limit (LOD) of the aluminosilica sensor/collector at all Si/Al ratios enables the possible detection of these target ions at nanomolar concentrations (Table 2) [13,30,44].

3.3. Adsorption performance of Cd(II) ion-sensor/collector system

The Langmuir equilibrium isotherm was applied in the study of the adsorption performance of Cd(II) ion removal from an aqueous solution using a mesosensor/collector. The monolayer coverage and removal characteristics of Cd(II) ions on a mesocollector surface at constant temperature is represented by the Langmuir isotherm (Fig. 6A and B) according to the following equation [40,45,46]:

$$\frac{C_e}{q_e} = \frac{1}{(K_L q_m)} + \left(\frac{1}{q_m}\right) C_e$$

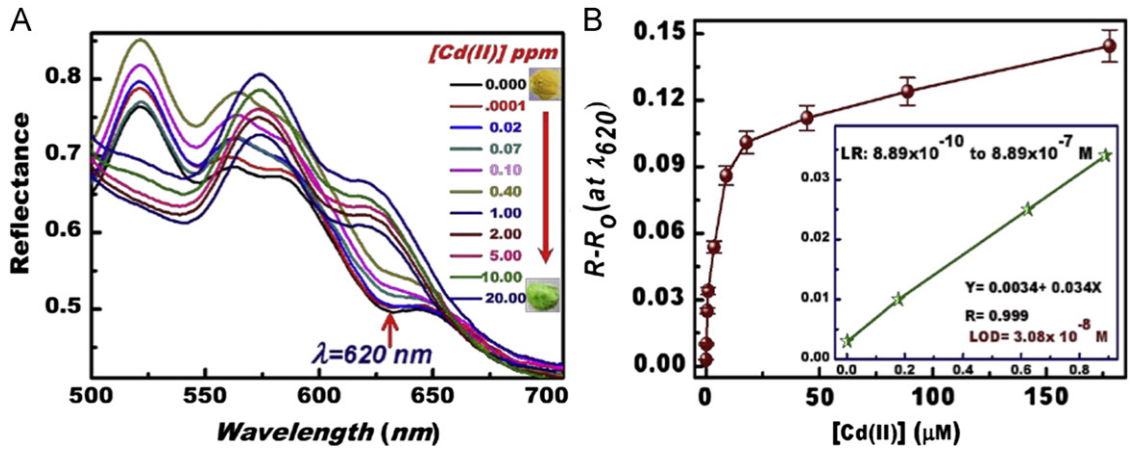

Fig. 5. Concentration-dependent changes in the UV/vis reflectance spectroscopic responses of aluminosilica mesocollectors (fabricated with Si/Al ratio of 9) during the recognition of Cd(II) (A) ions, calibration curve of Cd(II) ions (B) at optimal conditions (pH of 9.5, mesocollector amount of 20 mg, volume of 20 mL, t_R of 3 min, and temperature of 25 °C). The reflectance spectra of the [Cd-TMPyP]$^{n+}$ complexes was measured at λ_{max} of 620 nm.

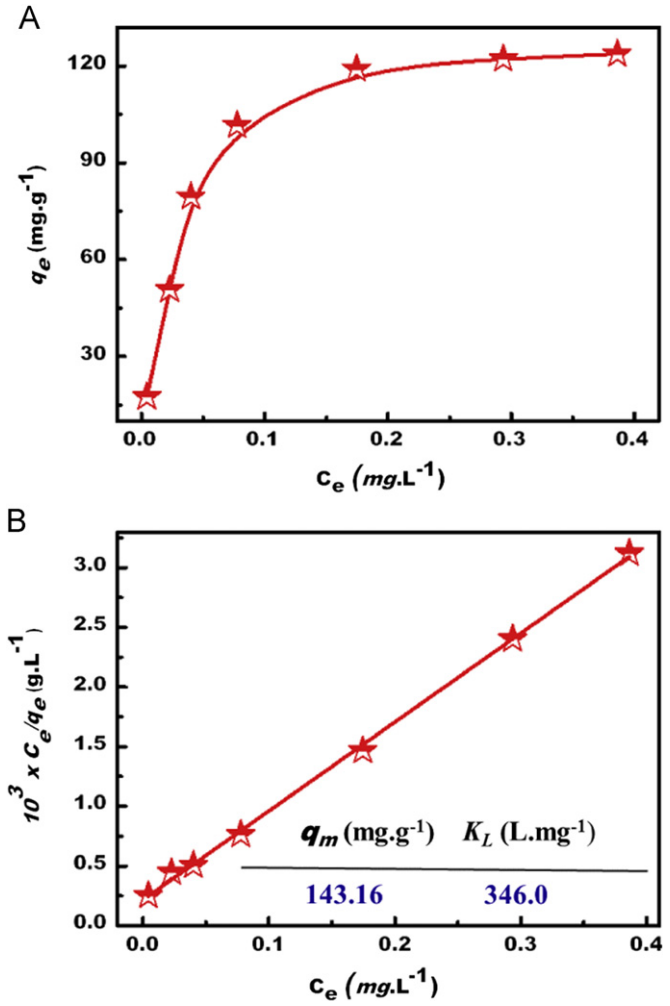

Fig. 6. Langmuir adsorption isotherms (A) and the linear form of the Langmuir plot (B) for the adsorption of Cd(II) analyte ions using aluminosilica mesocollectors (fabricated with Si/Al ratio of 9).

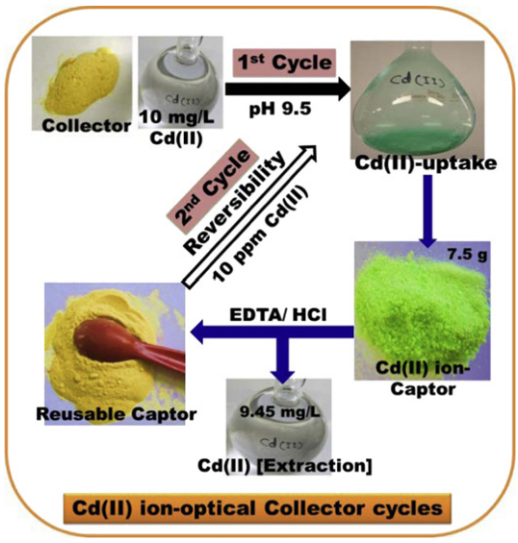

Scheme 2. Color profile of the TMPyP-modified-aluminosilicate mesocollector with the recovery/extraction system of [10 ppm] Cd(II) ions after several reuse/cycles (No.)

where q_m (mg g^{-1}) is the amount of Cd(II) metal ions removed to form a monolayer coverage and K_L is the Langmuir adsorption equilibrium constant. The monolayer coverage can be obtained from a plot of C_e/q_e versus C_e (Fig. 6B), which gives a straight line indicating the formation of the monolayer coverage of the Cd(II) ions in the interior pore surfaces of mesoporous aluminosilica collectors with these removal assays. The practical adsorption capacity q_m and the Langmuir coverage constant K_L were obtained from the slope and the intercept of the linear plot, respectively. The linear removal curves indicate that a wide range of Cd(II) ion concentrations can be removed from aqueous water in a one-step treatment with high adsorption efficiency of 96–99% (Scheme 2). These results indicate that the practical removal of 1 g of Cd(II) metal ions from an aqueous solution requires ~7.5 g of mesocollector. Our mesocollector shows significant adsorption efficiency over adsorbents, which also require intensive design and experimental conditions during the adsorption and assessment monitoring of Cd(II) ions.

3.4. Controlled Cd(II) ion-selective mesocollectors

A major advantage of the TMPyP-collector is its ability to create selective extraction systems for Cd(II) ions, thus preventing hindrance from actively interfering components, particularly the competitive element ions [33a,36,44]. These interfering components

may make the recovery of Cd(II) target ions from a mixture containing most competitive components difficult. To investigate the effect of interfered ions on the ion-selective collectors for Cd(II) ions, the interfered cations and anions were initially added to the nanocollector (Fig. 7) at ion-sensing conditions (pH 9.5, sensor amount of 20 mg, t_R of 3 min, volume of 20 ml, and temperature of 25 °C). This study was carried out by examining the effect of each interfering metal ion separately followed by its effect as groups (Fig. 7). The results showed that no significant changes in the visible color patterns and the reflectance spectra of the collector (blank solid sensor-TMPyP) at 620 nm were observed. Among all possible interfering cation species, the Cu^{2+} and Hg^{2+} ions at high concentration showed slight changes in both color map and reflectance intensities of the complexes, indicating a disturbance in the Cd(II) ion sensing systems. Fig. 7 shows the effects of various foreign surfactants and anions such as SDS, CTAB, Triton X-100, tartrate, citrate, oxalate, chloride, acetate, nitrite, nitrate, sulfite, sulfate, phosphate, and carbonate on the aluminosilica collectors under similar experimental conditions. Results indicate that the added surfactants and anions do not interfere with the Cd(II) ion collectors.

3.5. Applicability and the accuracy of the proposed Cd^{2+} ion-mesocollector sensor

In the point of view of customer relationship management systems, successful implementation, and use of the developed mesocollector sensor in real applicability can provide a significant advantage to the user. To assess the practical utility of the optical mesocollector sensor in terms of the quality and efficiency during the recognition of Cd^{2+} analyte from the commercial wastes, the quantification of 20 μg dm^{-3} levels of Cd^{2+} ion was investigated with pretreated real sample effluents collected from different sources such as food processing, hospital effluent, and manufacturing industries of semiconductor and Quartz (Table 3). The quantitative analyses of the sensor, according to the calibration plot (Fig. 5B), showed the detectable amounts to be 19.7–20.1 μg dm^{-3} for Cd^{2+} ions, with a standard deviation value of ≤ 3–4% for triplicate analyses. These analytical data indicated that the proposed sensing system of optical mesocollector can serve as a potential candidate for monitoring of Cd^{2+} ion from polluted environment.

3.6. Effective Cd(II) mesocollector reusability

To study the reusability of sensors for Cd(II) ion-sensing systems, simple treatment procedures using a specific concentration of EDTA or HCl (0.1 M) as a stripping agent were conducted for Cd(II) ion removal (i.e., decomplexation) after the solid sensor was collected from the sensing assays [13,40]. These releasing experiments were performed several times through a liquid-exchange process to release the Cd(II) ions and to obtain "Cd-free" sensor surfaces. These eluents have high binding affinity to form a more stable Cd(II) complex onto solid sensors compared with the Cd(II)-TMPyP complex. After multiple regeneration/reuse cycles (i.e., ≥ 6), the Cd(II) ion-sensing systems of the regenerated sensors showed a slight influence on the sensitivity with increased recovery time (t_R) of Cd-to-TMPyP binding events (Table 2). A well-controlled signaling in the quantification

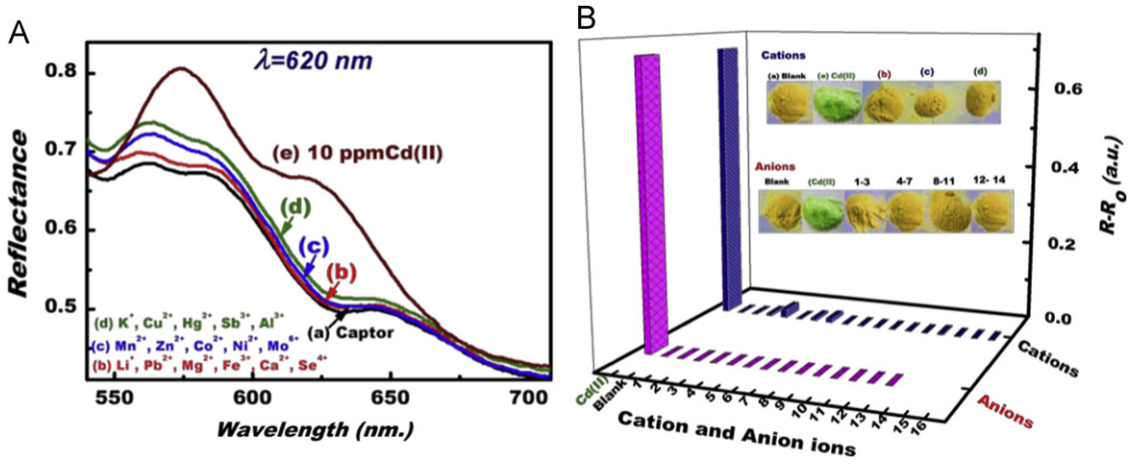

Fig. 7. Effect of the anions and the cations as interference ions on the absorbance spectra of the Cd-TMPyP complex formed during the detection of Cd (II) ion at [10 ppm] using the aluminosilica mesocollectors (fabricated with Si/Al ratio of 9). Note that the interfered cations from 1 to 16 are as follows; (1) Li^{2+}, (2) Co^{2+}, (3) Cu^{2+}, (4) Mo^{6+}, (5) Zn^{2+}, (6) Hg^{2+}, (7) Ca^{2+}, (8) Mg^{2+}, (9) K^{+}, (10) Fe^{3+}, (11) Pb^{2+}, (12) Mn^{2+}, (13) Al^{3+}, (14) Sb^{3+}, (15) Ni^{2+}, and (16) Se^{4+}. The interfered anions from 1 to 13 are as follows: (1) CTAB, (2) Triton X, (3) $C_8H_4O^{4-}$, (4) $C_6H_5O_7^{3-}$, (5) $C_2O_4^{2-}$, (6) CH_3COO^{-}, (7) NO_2^{-}, (8) NO_3^{-}, (9) SO_3^{2-}, (10) SO_4^{2-}, (11) CO_3^{2-}, (12) and PO_4^{3-}. The selectivity studies of Cd(II) ion-mesosensor/collector were studies at optimal conditions (pH of 9.5, mesocollector amount of 20 mg, volume of 20 mL, t_R of 3 min, and temperature of 25 °C).

Table 3
Analysis of Cd^{2+} in spiked environmental samples with optical mesocollector sensor fabricated by using cubic Ia3d aluminosilica mesostructures with Si/Al ratio of 4 as a platform.

Sample Source	Sample composition (mg dm^{-3})	Cd^{2+} spiked amount (ppb)	Cd^{2+} analyzed amount (ppb)
Hospital effluent	100—Na^{+}, K^{+}, Mg^{2+}, 1.75—Cu^{2+}, Ni^{2+}, Zn^{2+}, Fe^{2+}; 20—Ca^{2+},	20	19.7 ± 4.0*
Quartz discharge	0.1—La^{3+}, Ce^{4+}, Nd^{3+}, Sm^{3+}; 1.5—W^{6+}, Mo^{6+}, Mn^{2+}; 10—Ca^{2+}, Mg^{2+}, 0.5—Si^{4+}; 0.15—Bi^{3+}, Al^{3+}, Tl^{+}, Ga^{3+}, Ir^{3+}	20	19.7 ± 3.2
Semiconductor facility effluent	Nd^{3+}, Sm^{3+}; 1.0—W^{6+}, Mo^{6+}; 10—Ca^{2+}, Mg^{2+}; 0.75—Mn^{2+}, Si^{4+} 0.25—Bi^{3+}, Al^{3+}, Tl^{+}, Ga^{3+}, Ir^{3+}; 0.1—La^{3+}, Ce^{4+}	20	20.1 ± 3.0
Food processing	$As^{3+/5+}$, Mn^{2+}; 0.2—Sn^{2+}, Sb^{2+}; 10—Ca^{2+}, 1.5—Cu^{2+}, Ni^{2+}, Zn^{2+}, Fe^{2+}; 0.05—$Cr^{3+/6+}$, Mg^{2+}	20	20.3 ± 3.2

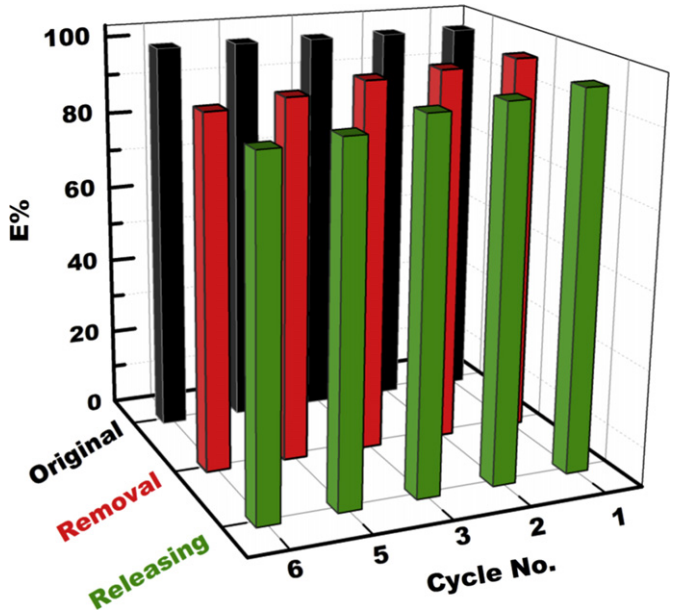

Fig. 8. ICP-AES analysis of the Cd(II) ion solution after completing all stages of the collector assays in terms of the removal and release of Cd(II) ions within multiple reuse cycles (No. ≥ 6). E% represents the percentage ratio of the Cd(II) concentration per reuse cycle (No.) of the initial concentration used (10 ppm) in collecting condition assays (recovery time > 60 min, amount of 30 mg, volume of 1 L, and temperature of 25 °C).

and detection of Cd(II) ions was attained, which indicated the stability of the TMPyP-modified aluminosilica sensors, as evidenced by the UV–Vis spectroscopic studies. Furthermore, the XRD pattern and N_2 isotherm (Fig. 1Ac and Bc) revealed the retention of ordered mesostructures and physical properties up to a high extent after several reuse/cycles.

A major advantage of mesocollectors is their retaining functionality in terms of Cd(II) ion recovery after multiple reuse cycles [47–49]. To investigate the efficiency of the collector design in Cd(II) ion recovery after several recovery cycles, the ICP-AES results of the Cd(II) ion solution were analyzed after all stages of the collector assays were completed according to the following (Scheme 2): (1) the removal of the Cd(II) ion from the aqueous solution and (2) the release of the Cd(II) ion from the solid collector (Fig. 8). The collector's signal intensity with each reuse cycle was compared with its signal spectra prior to the use of the stripping agent (EDTA). Analyses of the solid sample and the Cd(II) ion solution indicated that the collector had a well-controlled signaling in the recovery of Cd(II) ions even after multiple reuse cycles (No. ≥ 6) (Fig. 8). This finding indicated that the functional molecular probe onto the mesocollectors still attained its electron acceptor/donor strength functionality to offer effective binding and collection of the Cd(II) ion targets, despite the substantial influence upon cycling.

4. Conclusions

Mesocage cubic Ia3d aluminosilica collectors enable the construction of probe surface-mounted naked-eye ion-sensor strips for highly sensitive responses to the selective removal and sensitive recognition of Cd(II) target ions down to nanomolar concentrations. The use of aluminosilica-based platforms as selective mesopore shape and size carriers leads to the simple fabrication and stable design of optical sensors through the direct functionalization of TMPyP chelate with prior modifications of the surface materials. Within such a tailored mesocollector design, the ability to achieve flexibility in the specific activity of the electron acceptor/donor strength of the chemically responsive TMPyP molecular probe enables the easy generation and transduction of an optical signal as a response to TMPyP-Cd(II) binding events, even at ultra-trace concentrations of Cd(II) ions. Controlled sensing and removal assays significantly enhance mesocollector functionality in terms of long-term stability, reversibility, and selectivity. The key result in our study is that the design-made mesocollector can be used as effective tools for urban mining development, which are secondary resources in industrial countries.

Appendix A. Supplementary Information

Supplementary data associated with this article can be found in the online version at http://dx.doi.org/10.1016/j.talanta.2012.06.046.

References

[1] S. Sthiannopkao, S. Sreesai, J. Environ. Manage. 90 (2009) 3283–3289.
[2] F. Xiao, J.-C.H. Huang, J. Environ. Manag. 90 (2009) 3105–3109.
[3] F. Turner, Science 290 (2000) 1315.
[4] P. Chen, C. He, J. Am. Chem. Soc. 126 (2004) 728.
[5] M. Miro, J.M. Estela, V. Cerda, Talanta 63 (2004) 201.
[6] G. Aragay, J. Pons, A. Merkoc, Chem. Rev. 111 (2011) 3433–3458.
[7] G.D. Christian, Analytical Chemistry, 6th ed., John Wiley & Sons Inc., NY, 2003.
[8] C.T. McMurray, J.A. Tainer, Nat. Genet. 34 (2003) 239.
[9] J. Goel, K. Kadirvelu, C. Rajagopal, V.K. Garg, Ind. Eng. Chem. Res. 45 (2006) 6531.
[10] (a) T. Gunnlaugsson, T.C. Lee, R. Parkesh, Org. Lett. 5 (2003) 4065;
(b) M.H. Lee, K.K. Cho, A.P. Shah, P. Biswas, Environ. Sci. Technol. 39 (2005) 8481.
[11] A.A. Ensafi, Z.N. Isfahani, J. Anal. Chem. 66 (2011) 151–157.
[12] P. Andrewes, W.R. Cullen, E. Polishchuk, Environ. Sci. Technol. 34 (2000) 2249–2253.
[13] (a) S.A. El-Safty, A. Ismail, H. Matsunaga, F. Mizukami, J. Phys. Chem. 112 (2008) 4825–4835;
(b) S.A. El-Safty, A.A. Ismail, H. Matsunaga, T. Hanaoka, F. Mizukami, Adv. Funct. Mater. 18 (2008) 1485–1500;
(c) S.A. El-Safty, D. Prabhakaran, A.A. Ismail, H. Matsunaga, F. Mizukami, Chem. Mater. 20 (2008) 2644–2654.
[14] (a) M. Comes, M.D. Marcos, F. Sancenon, J. Soto, L. Villaescusa, A. Amoros, P.D. Beltran, Adv. Mater. 16 (2004) 1783–1786;
(b) A.B. Desacalzo, K. Rurack, K.H. Weisshoff, R.M. Manez, M.D. Marcos, P. Amoros, K. Hoffmann, J. Soto, J. Am. Chem. Soc. 127 (2005) 184–200.
[15] (a) A. Corma, Chem. Rev. 95 (1995) 559;
(b) A. Corma, Chem. Rev. 97 (1997) 2373–2420;
(c) A. Corma, M.S. Grande, V.G. Alfaro, A.V. Orchilles, J. Catal. 159 (1996) 375–382.
[16] D. Dubé, S. Royer, D.T. On, F. Béland, S. Kaliaguine, Micro. Meso. Mater. 79 (2005) 137.
[17] (a) Y. Wang, N. Lang, A. Tuel, Micro. Mesop. Mater. 93 (2006) 46;
(b) S.A. El-Safty, M.A. Shenashen, M. Khairy, M. Ismeal, Chem. Commun. 48 (2012) 6708–6710;
(c) S.A. El-Safty, M.A. Shenashen, M. Khairy, M. Ismeal, Adv. Funct. Mater. (2012)http://dx.doi.org/10.1002/adfm.201200393.
[18] A. Corma, S. Iborra, S. Miquel, J. Primo, J. Catal. 161 (1996) 713–719.
[19] S. Biz, M.G. White, J. Phys. Chem. B 103 (1999) 8432–8442.
[20] H. Hamdan, W. Zhou, J. Klinowski, J. Phys. Chem. 99 (1995) 1018–1024.
[21] Y. Zhang, X. Shi, J.M. Kim, D. Wu, Y. Sun, S. Peng, Catal. Today 93–95 (2004) 615–618.
[22] (a) M. Trueba, S.P. Trasatti, Eur. J. Inorg. Chem. 17 (2005) 3393–3403;
(b) D.L. Trimm, A. Stanislaus, Appl. Catal. 21 (1986) 215–238;
(c) Z.Y. Yuan, T.Z. Ren, A. Vantomme, B.L. Su, Chem. Mater. 16 (2004) 5096.
[23] P. Kim, J.B. Joo, H. Kim, W. Kim, Y. Kim, I.K. Song, J. Yi, Catal. Lett. 104 (3) (2005) 181–189.
[24] (a) S.A. El-Safty, A. Shahat, K. Ogawa, T. Hanaoka, Micro. Meso. Mater. 138 (2011) 51–62;
(b) S.A. El-Safty, M. Khairy, M. Ismeal, Sens. Act. B. Chemical 166–167 (2012) 253–263.
[25] (A) S.A. El-Safty, A. Shahat, Md.R. Awual, J. Colloid Interface Sci. 359 (2011) 9–18;
(B) S.A. El-Safty, A. Shahat, M. Ismael, J. Hazard. Mater. 201–202 (2012) 23–32.
[26] (a) A.R. Garcia, R.B. de Barros, A. Fidalgo, L.M. Ilharco, Langmuir 23 (2007) 10164–10175;
(b) S.A. EL-Safty, Trends Anal. Chem. 30 (2011) 447–458;
(C) S.A. EL-Safty, A. Shahat, W. Warkocki, M. Ohnuma, Small 7 (2011) 62–65.

[27] (a) C. Marquez-Alvarez, N. Zilkova, J. Perez-Pariente, J. Cejka, Catal. Rev. 50 (2008) 222–286;
(b) N. Bejenaru, C. Lancelot, P. Blanchard, C. Lamonier, L. Rouleau, E. Payen, F. Dumeignil, S. Royer, Chem. Mater. 21 (2009) 522–533.
[28] (a) Y. Lui, W. Zhang, T.J. Pinnavaia, Angew. Chem., Int. Ed. 40 (2001) 1255–1258;
(b) H. Du, V.V. Terskikh, C.I. Ratcliffe, J.A. Ripmeester, J. Am. Chem. Soc. 124 (2002) 4216–4217.
[29] S.A. El-Safty, A.A. Ismail, A. Shahat, Talanta 83 (2011) 1341–1351.
[30] S.A. El-Safty, J. Mater. Sci. 44 (2009) 6764–6774.
[31] Y. Li, J. Zhou, C. Liu, H. Li, J. Mater. Chem. 22 (2012) 2507–2511.
[32] Y. Xu, L. Zhao, H. Bai, W. Hong, C. Li, G. Shi, J. Am. Chem. Soc. 131 (2009) 13490–13497.
[33] (a) M.C. Aragoni, M. Arca, F. Demartin, F.A. Devillanova, F. Isaia, A. Garau, V. Lippolis, F. Jalali, U. Papke, M. Shamsipur, L. Tei, A. Yari, G. Verani, Inorg. Chem. 41 (2002) 6623;
(b) M. Bossi, V. Belov, S. Polyakova, S.W. Hell, Angew. Chem. Int. Ed. 45 (2006) 7462.
[34] X. Liu, T. Peng, J. Yao, H. Lv, C. Huang, J. Solid State Chem. 183 (2010) 1448–1456.
[35] (a) S.A. El-Safty, D. Prabhakaran, Y. Kiyozumi, F. Mizukami, Adv. Funct. Mater. 18 (2008) 1739–1750;
(b) S.A. El-Safty, A. Ismail, H. Matsunaga, F. Mizukami, Chem. Eur. J. 13 (2007) 9245–9255.
[36] (a) C.F. Chow, M.H.W. Lam, W.Y. Wong, Inorg. Chem. 43 (2004) 8387;
(b) J.V.R. Lis, M.D. Marcos, R.M. Mánez, K. Rurack, J. Soto, Angew. Chem. Int. Ed. 44 (2005) 4405–4407.
[37] X. Ji, Q. Hu, J.E. Hampsey, X. Qiu, L. Gao, J. He, Y. Lu., Chem. Mater. 18 (2006) 2265.
[38] (a) J.R. Matos, M. Kruk, L.P. Mercuri, M. Jaroniec, L. Zhao, T. Kamiyama, O. Terasaki, T.J. Pinnavaia, Y. Liu, J. Am. Chem. Soc. 125 (2003) 821;
(b) F. Kleitz, D. Liu, G.M. Anilkumar, I. Park, L.A. Solovyov, A.N. Shmakov, R. Ryoo, J. Phys. Chem. B 107 (2003) 14296.
[39] M.N. Timofeeva, V.N. Panchenko, A. Gil, A. Yu Chesalov, T.P. Sorokina, V.A. Likholobov, Appl. Catal. B-Environ. 102 (2011) 433–440.
[40] (a) S.A. El-Safty, T. Balaji, H. Matsunaga, T. Hanaoka, F. Mizukami, Angew. Chem. Int. Ed. 45 (2006) 7202;
(b) J.R. Matos, M. Kruk, L.P. Mercuri, M. Jaroniec, L. Zhao, T. Kamiyama, O. Terasaki, T.J. Pinnavaia, Y. Liu, J. Am. Chem. Soc. 125 (2003) 821;
(c) S.A. El-Safty, D. Prabhakaran, A. Ismail, H. Matsunaga, F. Mizukami, Adv. Funct. Mater. 17 (2007) 3731–3745.
[41] N.A. Carrington, G.H. Thomasa, D.L. Rodmana, D.B. Beach, Z.-L. Xue, Anal. Chim. Acta 581 (2007) 232.
[42] E. Palomares, R. Vilar, A. Green, J.R. Durrant, Adv. Funct. Mater. 2 (2004) 111.
[43] E.B. Sandell, Colorimetric Determination of Traces of Metals, 3rd ed., Interscience Publisher, INC., NY, 1959, P326.
[44] U.C. Saha, B. Chattopadhyay, K. Dhara, S. Kumar Mandal, S. Sarkar, A.R. Khuda-Bukhsh, M. Mukherjee, M. Helliwell, P. Chattopadhyay, Inorg. Chem. 50 (4) (2011) 1213–1219.
[45] G.G. Huang, J. Yang, Anal. Chem. 75 (2003) 2262–2269.
[46] S.J. Lee, S.S. Lee, J.Y. Lee, J.H. Jung, Chem. Mater. 18 (2006) 4713–4715.
[47] B.R. White, J.A. Holcombe, Talanta 71 (2007) 2015–2020.
[48] A. Yari, N. Afshari, Sens. Actuators B 119 (2006) 531–537.
[49] T. Leelasattarathkul, S. Liawruangrath, M. Rayanakorn, B. Liawruangrath, W. Oungpipat, N. Youngvises, Talanta 72 (2007) 126–131.